JACS
JOURNAL OF THE AMERICAN CHEMICAL SOCIETY
Article
pubs.acs.org/JACS

Mechanistic Elucidation of the Stepwise Formation of a Tetranuclear Manganese Pinned Butterfly Cluster via N−N Bond Cleavage, Hydrogen Atom Transfer, and Cluster Rearrangement

Clifton R. Hamilton,[§] Michael R. Gau,[§] Regina A. Baglia,[†] Sean F. McWilliams,[‡] and Michael J. Zdilla*

Department of Chemistry, Temple University, 1901 North 13th Street, Philadelphia, Pennsylvania 19122, United States

Supporting Information

ABSTRACT: A mechanistic pathway for the formation of the structurally characterized manganese-amide-hydrazide pinned butterfly complex, $Mn_4(\mu_3\text{-PhN-NPh-}\kappa^3N,N')_2(\mu\text{-PhN-NPh-}\kappa^2\text{-}N,N')(\mu\text{-NHPh})_2L_4$ (L = THF, py), is proposed and supported by the use of labeling studies, kinetic measurements, kinetic competition experiments, kinetic isotope effects, and hydrogen atom transfer reagent substitution, and via the isolation and characterization of intermediates using X-ray diffraction and electron paramagnetic resonance spectroscopy. The data support a formation mechanism whereby bis[bis(trimethylsilyl)amido]manganese(II) ($Mn(NR_2)_2$, where R = $SiMe_3$) reacts with *N,N′*-diphenylhydrazine (PhNHNHPh) via initial proton transfer, followed by reductive N−N bond cleavage to form a long-lived Mn^{IV} imido multinuclear complex. Coordinating solvents activate this cluster for abstraction of hydrogen atoms from an additional equivalent of PhNHNHPh resulting in a Mn(II)phenylamido dimer, $Mn_2(\mu\text{-NHPh})_2(NR_2)_2L_2$. This dimeric complex further assembles in fast steps with two additional equivalents of PhNHNHPh replacing the terminal silylamido ligands with η^1-hydrazine ligands to give a dimeric $Mn_2(\mu\text{-NHPh})_2(PhN\text{-}NHPh)_2L_4$ intermediate, and finally, the addition of two additional equivalents of $Mn(NR_2)_2$ and PhNHNHPh gives the pinned butterfly cluster.

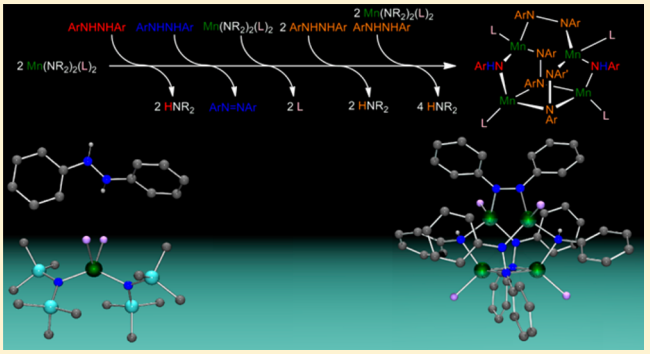

1. INTRODUCTION

An interest in the development of water oxidizing catalysts for the generation of renewable hydrogen has prompted new research into nature's sole water oxidizing catalyst, the oxygen evolving cluster (OEC) of photosystem II.[1−6] This cluster is a manganese−calcium−oxo heterocubane cluster with a fourth "dangler" manganese atom, a unique cofactor in biology. The structure shown in Figure 1 represents the X-ray crystallographic model of the OEC.[7] During turnover, the OEC undergoes a series of one-electron proton coupled electron transfer (PCET) events,[8] oxidizing it through the S-states of the Kok cycle[9] (Figure 2). From the S_4 state, the cluster evolves O_2 and relaxes to the S_0 state. There is a consensus that the OEC undergoes substantial geometric rearrangement throughout the

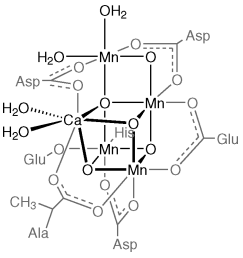

Figure 1. Crystallographic model of the oxygen evolving cluster.

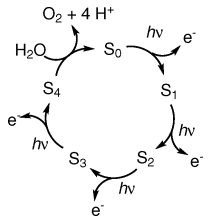

Figure 2. Kok cycle for water oxidation by the oxygen evolving cluster.

S-state cycle, based on X-ray absorption spectroscopy.[10] While the exact structures of the intermediates are not known, a number of proposals exist based upon Density Functional Theory studies.[11−13] Recently, femtocrystallography has given the first three-dimensional insights into the structure of Photosystem II in elevated S-states.[14]

There is a renewed interest in the synthesis of Mn−O clusters of late, including reports of two Mn−Ca clusters modeling the cubane core of the cluster from the groups of Agapie and Christou.[15,16] While the synthetic manganese-oxo model complexes are extensive (hundreds of reports),[17] actual chemical reactivity studies are rare due to the high stability of most models, which are chelated. Examples of well charac-

Received: August 11, 2014
Published: November 26, 2014

dx.doi.org/10.1021/ja508244x | J. Am. Chem. Soc. 2014, 136, 17974−17986

terized reactivity include oxygen atom transfer reactions,[18,19] reversible rearrangement,[20] water oxide incorporation[21] and O_2 evolution.[22,23]

The value of model complex chemistry is to obtain mechanistic understanding of the active sites of metalloproteins using simpler, easy-to-handle models. For example, model complexes of the OEC may serve as a means to scrutinize proton-coupled electron transfer and its effects on cluster rearrangement and reductive elimination mechanisms relevant to OEC turnover, as has been demonstrated, for example, in recent work on a mononuclear system by Borovik.[24] Yet to our knowledge, there have been no thorough mechanistic studies on these or any other reactions at any manganese cluster. The rearrangement of an iron-chalcogenide cluster into a P-cluster model is worthy of note, which was reported by Holm and co-workers, who showed that substituted selenides could be used to trace the movement of chalcogenide ligands during rearrangement.[25]

We reported previously the synthesis of the first structurally characterized pinned butterfly cluster of manganese.[26] The butterfly structure type is a proposed intermediate in an OEC model system and has been suggested to be a species of possible relevance to the OEC.[22] The reaction of bis[bis-(trimethylsilyl)amido]manganese(II) with 5 equiv of *N,N′*-diphenylhydrazine (PhNHNHPh) results in the formation of the all-Mn(II) pinned butterfly complex $Mn_4(\mu\text{-NHPh})_2(\mu_3\text{-PhNNPh-}\kappa^3N,N')_2(\mu\text{-PhNNPh-}\kappa^2N,N')(py)_4$ (**2**, L = THF, py) and an equivalent of azobenzene (eq 1).[26]

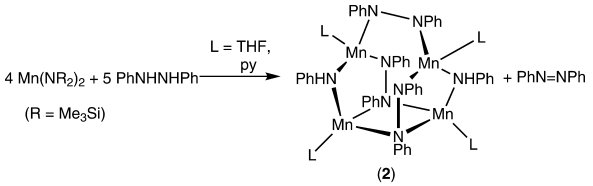

(1)

This reaction proceeds through a black intermediate which we refer to as **1a**. This black solution subsequently bleaches to give the orange-red suspension containing **2** in ca. 90% yield. Under alternate conditions of low temperature (−40 °C) and excess hydrazine, we have been able to isolate a pale pink heteroleptic dimer $Mn_2(\mu\text{-NHPh})_2(NR_2)_2L_2$ (**1b**) from the black mixture. We proposed in the original report[26] that this complex might be a side product, or an intermediate on the way to the formation of **2**.

The ligand set in **2** contains three intact, doubly deprotonated diphenylhydrazides, two phenylamido ligands which we presumed[26] to have formed via disproportionation of hydrazine to give the reduced amide ligands and oxidized azobenzene. The initial $^-NR_2$ ligands (R = Me_3Si) have been removed by protolysis to form HNR_2 (hexamethyldisilazane, HMDS), and the final cluster is terminally ligated by tetrahydrofuran (THF) or pyridine (py). Our initial report left a number of questions about this system unanswered: Why is one hydrazine cleaved, but three left intact? What is the mechanism of N−N bond activation? What is the identity of the intermediates, and in particular, the black **1a**? Is dimer **1b** an intermediate or a side product? In this report we address these questions and provide mechanistic information on this manganese cluster self-assembly reaction. The elucidated pathway mirrors key processes occurring at the OEC (oxidation by proton coupled electron transfer, cluster rearrangement, and O−O bond formation), albeit in reverse order in our system: N−N bond cleavage, reduction by proton-coupled electron transfer, with geometric cluster rearrangements throughout.

2. RESULTS AND DISCUSSION

2.1. Formation and Consumption of Intermediate 1a.

Kinetic monitoring by absorption spectroscopy in THF at 635 nm mirrors the visually observed formation of a black intermediate(s) over the course of a few minutes, and its subsequent disappearance over the course of ca. 4 h to give an orange-red solution. UV−visible spectral monitoring in the region of 400−700 nm shows the conversion to the black colored intermediate corresponding to a broad band with a maximum around 610 nm, tailing into the infrared region over the first 2 min of the reaction. Subsequently, the disappearance of this dark intermediate is observed as this broad absorption band decays over the course of several hours (Figure 3).

A kinetic trace at 635 nm (near the absorption difference maximum) clearly shows the appearance and decay of the dark colored intermediate. Upon close examination of the kinetic trace near the start of the reaction over the course of 10 min (Figure 3 inset) an initial induction period is apparent before the appearance of the black intermediate **1a**. This induction indicates either a product catalyzed (autocatalytic) reaction, or an initial slow step during which colorless Mn(II) oxidation states are maintained. The substitution of deuterated PhNDNDPh for PhNHNHPh demonstrates that the induction period possesses a substantial kinetic isotope effect, suggesting the involvement of the hydrazine hydrogen atom in early stages of the reaction, preceding N−N bond cleavage, and ruling out autocatalysis as the cause of the induction period. Additional experiments ruling out the possibility of autocatalysis are provided in the Supporting Information.

The proposed mechanism is the initial protolysis of NR_2 by PhNHNHPh to give HNR_2 and a colorless hydrazide complex, which then further reacts, cleaving the N−N bond and resulting in an oxidized black Mn-imide compound:

$$\mathrm{Mn(NR_2)_2 + PhN\mathbf{H}N\mathbf{H}Ph} \xrightarrow{k_1} \mathrm{Mn(PhN\text{-}N\mathbf{H}Ph)(NR_2) + \mathbf{H}NR_2} \quad (2)$$

$$\mathrm{Mn(PhN\text{-}N\mathbf{H}Ph)(NR_2)} \xrightarrow{k_2} \mathrm{Mn(PhN\text{-}NPh) + \mathbf{H}NR_2} \quad (3)$$

$$\mathrm{Mn(PhN\text{-}NPh)} \rightarrow \underset{(\mathbf{1a})}{\mathrm{Mn^{ox}(NPh)_2}} \quad (4)$$

In this proposal, the observed induction period results from the protolysis of NR_2 by hydrazine, leading to no initial color change (eq 2). The resulting colorless hydrazide adduct must accumulate to a reasonable extent before the kinetics of N−N bond cleavage reach their maximum at the inflection point of the curve (eq 4).

The observed kinetic isotope effect supports the involvement of the hydrazine proton in the first step of the reaction. Simulation of the kinetic trace reveals that two proton-dependent steps (eqs 2 and 3) are necessary to simulate the observed concentration profiles. These simulations (Figure 3) indicate a kinetic isotope effect of 23 ± 3 for the first protolysis step (eq 2) and 4.8 ± 0.3 for the second (eq 3). While the kinetic trace resulting from reaction of $Mn(NR_2)_2$ with protio-diphenylhydrazine has an excellent fit to simulation, the deutero-hydrazine trial is less ideal. This is due to the fact

dx.doi.org/10.1021/ja508244x | J. Am. Chem. Soc. 2014, 136, 17974−17986

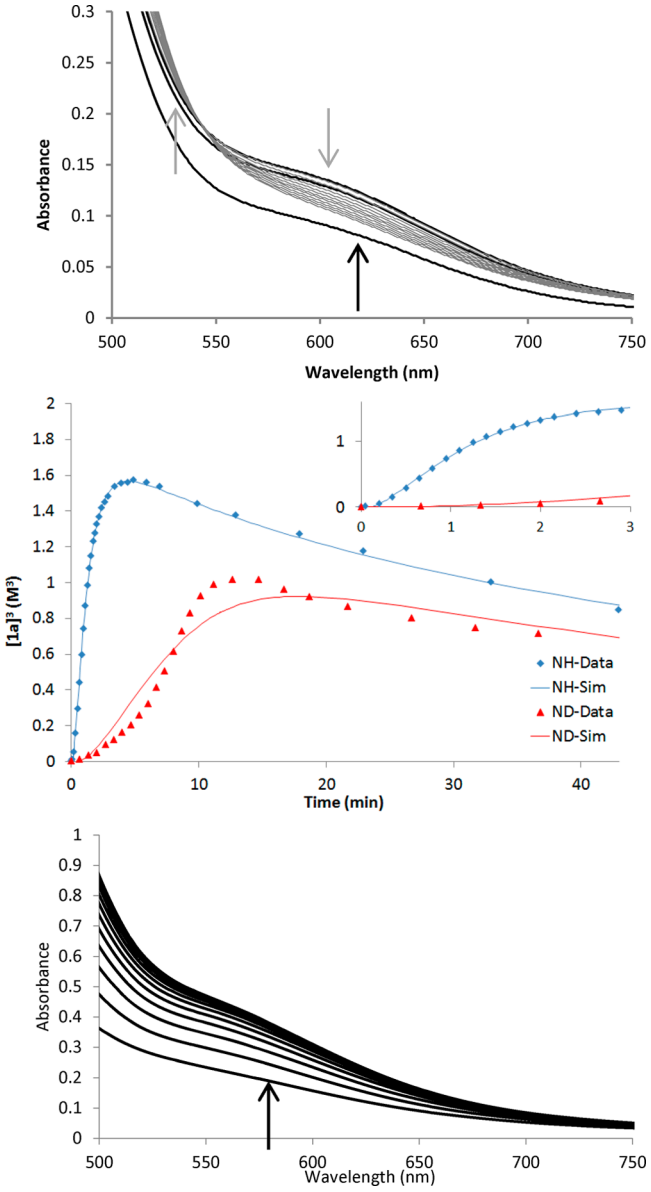

Figure 3. (Top) Spectral evolution of the reaction of bis[bis(trimethylsilyl)amido]manganese(II) with *N*,*N*′-diphenylhydrazine in THF. Initial appearance of **1a** is illustrated by the three bold, black spectra, followed by decay of **1a** to give **2**, shown in gray spectra with isosbestic point at 543 nm. (Middle) Absorption at 635 nm of the reaction of $Mn(NR_2)_2$ with PhNHNHPh showing the appearance and disappearance of black **1a**. Inset: expanded view of the first 10 min of reaction. Simulated traces are shown as solid lines. Concentrations were determined using the ε value of **1a** calculated from titration experiments (vide infra, section 2.2), assuming a tetranuclear cluster with formula $[Mn(NPh)_2]_4$; ε = 300 $M^{-1}cm^{-1}$. (Bottom) Spectral evolution of the reaction of $Mn_2(NHPh)_2(NR_2)_2(THF)_2$ (**1b**) and $Mn(NR_2)_2$ with PhNHNHPh (added last) in THF, showing direct formation of **2**. $[Mn(NR_2)_2]_0$ = 23.6 mM, $[PhNHNHPh]_0$ = 48.4 mM. Simulation parameters: (NH, fitted) k_1 = 42(3) M^{-1} s^{-1}, k_2 = 0.0167(3) s^{-1}, k_4 = 0.0216(4) M^{-1} s^{-1}, (ND, fitted) k_1= 1.8(2) M^{-1} s^{-1}, k_2 = 0.00346(18) s^{-1}, k_4 = 0.017(3) M^{-1} s^{-1}, (fixed) k_d = 0.837 s^{-1}, k_{-d} = 25.4 s^{-1}, k_3 = 9.89 s^{-1}, k_{-3} = 4.43 s^{-1} (see Scheme 5 for rate constant definitions).

that there is actually more than one black intermediate during the hydrogen atom transfer (HAT) phase of the reaction. The presence of additional intermediates distort the curvature of the experimental kinetic trace away from our simple model in the case of the experiment with deuterated hydrazine. This is discussed further in the Supporting Information.

A further test of early protolysis was carried out by the use of methylated hydrazine, i.e., *N*,*N*′-dimethyl-*N*,*N*′-diphenylhydrazine (PhNMeNMePh), in place of PhNHNHPh. The only likely reactivity difference in this substrate compared with PhNHNHPh is its inability to transfer a proton to R_2N^-. Mixing of PhNMeNMePh with $Mn(NR_2)_2$ results in no reaction whatsoever. This result supports the proposal that initial protolysis of NR_2^- is required, and that coordination of deprotonated hydrazine precedes N−N bond cleavage.

In addition to the rate dependence on the initial protolysis step, there is a significant rate dependence on ligand field strength of the solvent (arene < THF < pyridine). In contrast to the reaction carried out in THF (data shown in Figure 3), the reaction in pyridine results in a much slower change to black, and the reaction in non-ligating arene solvents (benzene or toluene) results in an immediate change to black not able to be kinetically monitored by a standard apparatus. Similarly, there is an inverse rate dependence on concentration of donor solvent (Supporting Information).

$M(NR_2)_2$ complexes are known to form equilibrium adducts with ligating solvents.[26,27] The rate dependence on solvent donor ability is proposed to be a result of a ligand dissociation step preceding hydrazine coordination, leading to faster reaction in weakly ligating solvents. In the case of pyridine, the initial ligand dissociation is slow enough that steady state conditions are reached early, and no induction period is observed. The dependence of reaction rate on solvent concentration has been assessed by performing the reaction in the presence of varying amounts of THF. The kinetic data (see Supporting Information, Figure S2) clearly show the inhibition of the reaction by ligating solvent, suggesting a simple dissociative mechanism for the replacement of a solvent ligand by PhNHNHPh:

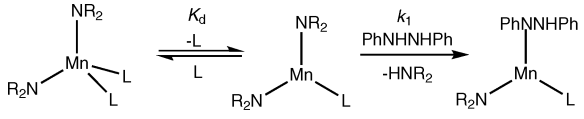

(5)

2.2. Identity of Intermediary 1a. The intense color of the intermediate **1a** (in comparison to the pale or colorless, high-spin Mn(II)-N species normally isolated) suggests that the decomposition of the Mn(II)-hydrazide adduct (previous section) results in oxidized manganese centers with allowed d-d transitions. The simplest explanation is the reductive cleavage of the N−N bond to give higher oxidation state (III or IV) Mn-imides. Difference infrared (DIR) spectroscopy in the N−H stretching region shows the initial disappearance of hydrazine N−H peaks to give an intermediate with no N−H peaks, and after 20−30 min, the gradual appearance of the N−H signal of **2** (Figure 4). The DIR spectroscopy therefore suggests that intermediary **1a** does not contain N−H protons, consistent with our previous report of its Fourier transform infrared (FTIR) spectrum.[26]

We maintain our initial hypothesis that black **1a** is an oxidized Mn-imido species which further reacts with hydrazine to be reduced back to a Mn(II)-amide with concomitant formation of azobenzene. However, we have discovered that the reactivity of **1a** is remarkably solvent dependent. As previously reported[26] and as described in section 2.1, black **1a** forms over the course of minutes in THF (or pyridine) and

dx.doi.org/10.1021/ja508244x | J. Am. Chem. Soc. 2014, 136, 17974−17986

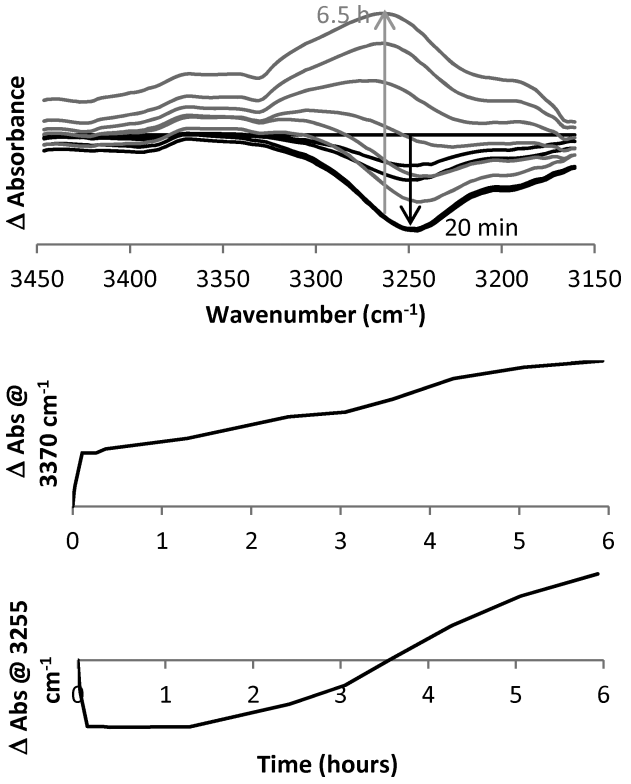

Figure 4. (Top) DIR spectra in the N−H stretch region monitoring the formation of **1a** from $Mn(NR_2)_2$ (61 mM) and PhNHNHPh (82 mM), and its further reaction to form **2** in pyridine. The disappearance of the N−H band of PhNHNHPh (black, negative peaks at 3250 cm^{-1}) occurs over the course of 20 min, and the appearance of the N−H stretches of **2** (gray, positive peaks at 3263 cm^{-1}) over the course of the next 6.5 h. The N−H stretch of hexamethyldisilazane appears immediately (3370 cm^{-1}), and grows throughout the reaction. (Middle) Kinetic trace of Δ absorbance at 3370 cm^{-1} (hexamethyldisilazane peak). (Bottom) Kinetic trace of Δ absorbance at 3255 cm^{-1}. Both kinetic traces show similar topology to kinetic traces by UV−vis (Figure 3).

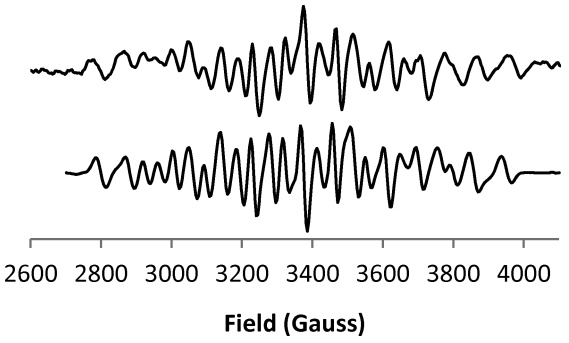

Figure 5. Baseline-corrected EPR spectra. (Top) $[\mathbf{1a}]^-$ after reduction of **1a** by one electron using $Na[COPh_2]$. (Bottom) Freeze-quenched solution during synthesis of **2a**. See Supporting Information, Figure S8, for uncorrected spectra.

further reacts to an orange (in THF) or red (in Py) solution over the course of hours. In non-coordinating solvents such as benzene, however, the solution turns ink-black instantaneously (faster than the rate of mixing under synthetic conditions), and remains black. Although presumed to be the same species as that formed in THF, **1a**, when formed in non-ligating solvent reacts slowly or not at all with hydrazine or other proton coupled electron transfer (PCET) reducing agents such as 2,6-di-*tert*-butylphenol or 9,10-dihydroanthracene (DHA). Thus, the role of coordinating solvent in the speciation of manganese is relevant not only to the formation of **1a** (see previous section 2.1), but to its reactivity as well.

While we can isolate **1a** in a benzene-solvated reaction mixture, attempts to crystallize black **1a** have been unsuccessful due to its hypersolubility in even the most nonpolar solvents (pentane, hexamethyldisiloxane). Reaction of $Mn(NR_2)_2$ with phenyl azide did not give this product, instead forming an insoluble tan powder, and attempts to trap and derivatize **1a** with chelating ligands have also not been successful. Despite having no measurable magnetic susceptibility by Evans method, the material is also NMR silent. This may be due to the combination of population of low-lying excited magnetic states at room temperature (common for weak-field $S = 0$ metal clusters)[28−32] as well as oligomerization in solution (vide infra), both of which broaden NMR signatures.

Despite these challenges, some features of this material may be gleaned using other experiments. Generation of a Job plot using electronic absorption spectroscopy demonstrates that $Mn(NR_2)_2$ and PhNHNHPh react in a 1:1 stoichiometric ratio to form **1a** (Figure S4). This result narrows the possibilities for **1a** to products of a 1:1 reaction. The two acidic hydrazine protons protolytically remove the NR_2 ligands as HNR_2, leading to an empirical Mn(PhN-NPh) complex. The protolysis of both $[NR_2]^-$ ligands is supported by quantification of HNR_2 via ^1H NMR (70−85% yield). Mn(II) in this environment is sufficiently reducing to induce oxidative addition of the hydrazine ligand based on previous studies.[33] Oxidative addition would result in an empirical manganese bis(imido) complex, $Mn^{IV}(NPh)_2$.

Studies of colligative properties of solutions of **1a** suggest it is aggregated in solution. Measurement of the freezing point of an in situ solution of **1a** shows only enough freezing point depression to account for the formation of 2 equiv of HNR_2, thus indicating that **1a** is best described as coordination oligomers that contribute negligibly to colligative property measurements.

Electron paramagnetic resonance (EPR) analysis of a black **1a** formed in toluene with a slight excess of $Mn(NR_2)_2$ results in an EPR spectrum showing only speciated $Mn(NR_2)_2$ in the presence of ligands (Figure S8).[33] Thus, black **1a** is EPR silent, consistent with a multinuclear, antiferromagnetically coupled compound. The addition of a sub-stoichiometric amount of the one-electron reductant, sodium benzophenone ketyl ($Na[COPh_2]$), results in the appearance of an $S = {}^1/_2$ species observable at $g = 2$ (Figure 5). This species was not observed prominently when outer-sphere reductants (Na-naphthalene, Na(s)) were attempted, suggesting the reduction may occur via an inner-sphere process. This spin state is consistent with antiferromagnetic coupling common to metal imido clusters.[34−36] This EPR spectrum exhibits extensive splitting from manganese hyperfine interactions, far more than observed in the dimeric manganese *tert*-butyl imido dimer of Danopoulos and Wilkinson (13 lines).[34] The extensive splitting is more consistent with at least a tetranuclear cluster, though mixtures of larger clusters cannot be excluded.

2.3. Further Reaction of 1a with Hydrazine. In an analysis of the oxidation states of the final products, it is clear that 2 equiv of PhNHNHPh is ultimately disproportionated into azobenzene and the two reduced phenylamido ligands of **2**

dx.doi.org/10.1021/ja508244x | J. Am. Chem. Soc. 2014, 136, 17974−17986

(eq 1). Transition metal complexes are known to disproportionate hydrazines.[37−41] In particular, a fully elucidated mechanism for disproportionation of hydrazine at iron was reported by Holland et al., and occurred by a radical process, involving Fe(I) intermediates.[42,43] In the present study, experimental support of a Mn(IV) imido intermediate implicates HAT from additional hydrazine equivalents as the operative mechanism for generation of azobenzene, as this type of reactivity of terminal imido complexes is well-established.[44−48] However, in non-ligating solvents such as benzene and toluene, the reaction of intermediate **1a** with PhNHNHPh is sluggish. In the presence of ligating solvent such as pyridine or THF (whether added at the beginning of the reaction, or after the formation of **1a**), this black species becomes reactive, and bleaches in the presence of PhNHNHPh. Indeed, when THF and PhNHNHPh are added to a black mixture of **1a** in benzene, HAT resumes as evidenced by the formation of azobenzene in approximately 97% yield (eq 6). In a crossover experiment where TolNHNHTol was added to **1a** as the HAT donor, the recovery of TolN═NTol was ∼60%. The metal based product of this reaction is an intractable yellow powder, which we presume to be a coordination polymer of $Mn(NHPh)_2$. This assignment is further supported by the observation that an intractable yellow powder that is identical based upon powder diffraction can be obtained from the reaction of $Mn(NR_2)_2$ with 2 equiv of aniline (eq 7). The putative $Mn(NHPh)_2$ can be further reacted with $Mn(NR_2)_2$ to form **1b** in low (∼20%) yield (eq 8).

$$[\underset{\textbf{(1a)}}{Mn^{IV}(NPh)_2}]_n + PhNHNHPh \xrightarrow{THF} [Mn^{II}(NHPh)_2]_n + PhN{=}NPh \quad (6)$$

$$Mn^{II}(NR_2)_2 + 2PhNH_2 \rightarrow [Mn^{II}(NHPh)_2]_n + 2HNR_2 \quad (7)$$

$$[Mn^{II}(NHPh)_2]_n + Mn^{II}(NR_2)_2 \rightarrow \underset{\textbf{(1b)}}{Mn^{II}_2(\mu\text{-}NHPh)_2(NR_2)_2} \quad (8)$$

The reactivation of **1a** by donor solvent is not successful with dried **1a**, suggesting that drying of **1a** irrevocably alters its identity.

An in situ EPR spectrum of the freeze-quenched reaction mixture of $Mn(NR_2)_2$ and PhNHNHPh in 2-methyl-THF exhibits a multiline signal during turnover equivalent to that observed when **1a** is reduced by a single electron donor (Figure 5), indicating the presence of an identical multinuclear species in the reaction mixture. The formation of the same multiline species by reduction of **1a** (whether by HAT, as here, or by addition of single-electron reductants) suggest this species is a likely reaction intermediate, and is consistent with the aggregated nature of **1a** as assessed by colligative property measurements (section 2.2).

We propose an equilibrium displacement of core imide bonds by ligating solvent, which activates **1a** for HAT, resulting in mixed-oxidation-state, EPR active species. The proposal is illustrated in Scheme 1 using a hypothetical geometry for **1a**. Activation of **1a** upon core rupture is plausible for two reasons: (1) An increase in reduction potential of Mn is expected resulting from replacement of a strong imido donor with a weaker solvent donor, increasing the favorability of HAT to **1a**. (2) The dissociation of the bridging imide from the positively

Scheme 1. Activation of Oligomeric 1a (Hypothetical Geometry) for Hydrogen Atom Transfer by Solvent Displacement of Core Bonding Interactions[a]

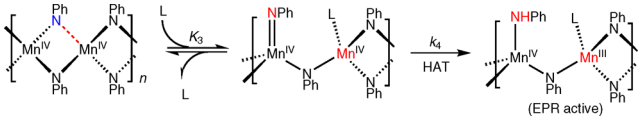

[a]Activated bonds and atoms are shown in red. Solvent L = THF or py.

Scheme 2. Kinetic Competition between Reaction of 1a with PhNHNHPh vs DHA

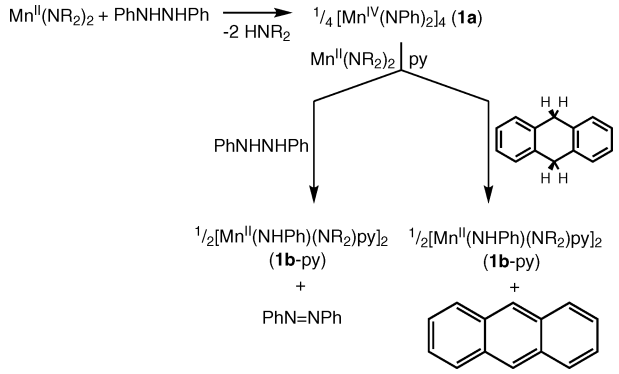

charged metal increases the basicity and steric accessibility of the N atom, activating it for HAT. Subsequent HAT reactions lead ultimately to the arrival at the 2+ Mn oxidation state, and phenylamido ligands present in the product **2**. An essentially identical mechanism for reversible core rupture of high-oxidation state manganese imido clusters by ligating solvent (pyridine) has been proposed to be responsible for core-terminal imido ligand isomerization in manganese *tert*-butyl imido systems.[34]

Support of the HAT mechanism by usual means such as pseudo-first-order kinetics and isotope effects are complicated by the initial rate-limiting proton transfer, and subsequent multiple-step processes. Instead, the propensity of intermediate **1a** to effect HAT reactions can be assessed by the inclusion of other hydrogen atom donors as kinetic competitors. In the presence of ligating solvent, intermediate **1a** is able to abstract C−H hydrogen atoms from DHA when included in the reaction mixture in excess. The abstraction of hydrogen from excess DHA is able to outcompete the abstraction of hydrogen from hydrazine due to the larger concentration of DHA. This results in a reaction mixture that remains lighter in color due to the rapid consumption of **1a** (Scheme 2). Significant quantities of anthracene are detected by gas chromatography and ^{1}H NMR (almost 100% yield based on Mn). Especially in light of the comparability of hydrazine N−H (73 kcal/mol)[49] bonds to DHA C−H bonds (78 kcal/mol),[50] HAT from DHA strongly suggests that reaction of **1a** via HAT from hydrazine is the most plausible mechanism of formation of azobenzene, and reduction of the manganese(IV) intermediates back to Mn(II). In the absence of ligating solvent, no anthracene is formed, confirming the role of ligating solvent in the activation of **1a** for HAT.

2.4. Assembly of Pinned Butterfly 2: Is 1b an Intermediate? Reaction of intermediate **1a** with PhNHNHPh by HAT results in Mn(II) and phenylamido ligands. Any number of subsequent assembly reactions may be responsible

dx.doi.org/10.1021/ja508244x | J. Am. Chem. Soc. 2014, 136, 17974−17986

for the conversion of **1a** to **2**. In our initial communication on the generation of **2**, we noted that a Mn(II)-phenylamido dimer, $Mn_2(\mu\text{-NHPh})_2(NR_2)_2(THF)_2$ (**1b**) was isolated under conditions of excess hydrazine and low temperature. A simple protocol for the synthesis of **1b** was also provided[26] via the reaction of 2 equiv of aniline with 2 equiv of $Mn(NR_2)_2$:

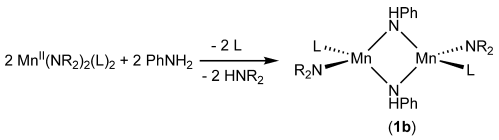

(9)

We proposed at this time that **1b** could be an intermediate in the assembly of **2**. The intermediate could form from the Mn^{II}–NHPh product of HAT by reaction with an equivalent of $Mn(NR_2)_2$:

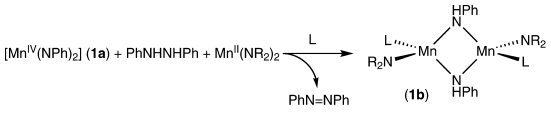

(10)

The notion that **1b** is an intermediate in the formation of **2** is an appealing proposal, as it would explain why in the formation of **2** one hydrazine is cleaved and three are not. The initial $Mn(NR_2)_2$ precursor is highly electron rich, having a low oxidation state (Mn^{II}), and strong silylamido donors. This electron-rich metal center would be expected to reductively cleave the N–N bond of hydrazine to give **1a**, which could then be reduced by HAT to give Mn(II)-amido species, such as **1b**. Dimer **1b**, now with a replacement of strongly donating silylamido ligands by the weaker arylamidos, may not have the reducing power to further cleave hydrazines, and so is expected to assemble with intact hydrazide ligands following protolytic replacement of the remaining silylamido ligands (Scheme 3).

Scheme 3

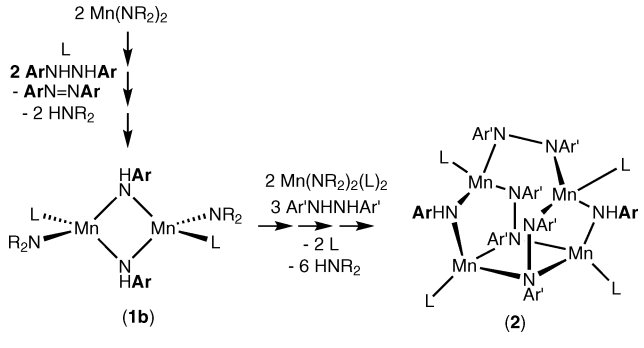

While the proposed reaction scheme shown in Scheme 3 explains the ligand stoichiometry of **2**, the potential problem with the proposal is that in order to explain the high yields, the final steps of this mechanism, the assembly of six molecules (one **1b**, three hydrazines, and two manganese precursors) to give **2** would have to be fast. The reason for this is that the two reagents reacting with **1b** (namely $Mn(NR_2)_2$ and ArNHN-HAr) annihilate each other in the first step, the formation of **1b**. The involvement of both of these reagents in both steps of the proposed assembly mechanism indicates that the final assembly step must be fast, rapidly consuming **1b** as it is formed, in order for the quantitative conversion to **2** evidenced by the high isolation yields.

Thanks to the drastically different colors of black, oxidized **1a** and the pale, reduced Mn(II) **1b** and **2**, this mechanism can easily be tested by a competition kinetics experiment. Under normal reaction conditions, $Mn(NR_2)_2$ and PhNHNHPh react to give the black intermediate **1a**, which is the source of reduced amide ligand in **1b**. However, if aniline is introduced first, this generates **1b** in situ, and provides the reduced amide ligand before the introduction of hydrazine. Thus, if the claim of fast assembly of **2** from **1b**, hydrazine, and $Mn(NR_2)_2$ is correct, the black intermediate **1a** will be circumvented, and the solution should turn immediately to the red color of **2**. If the fast assembly proposal is not true, the formation of **2** will proceed through the usual black intermediate. This competition kinetics experiment is illustrated in Scheme 4.

Scheme 4. Competition Experiment Testing Assembly of 1b with $Mn(NR)_2$ and PhNHNHPh in a Fast Step[a]

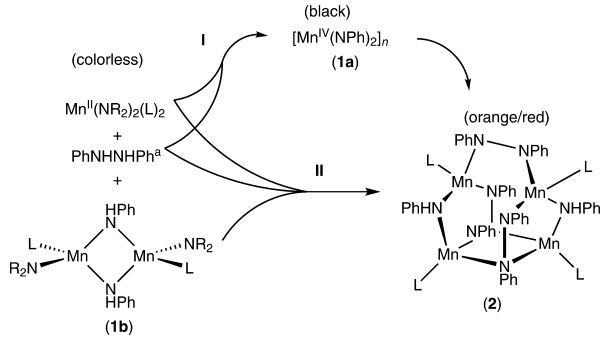

[a]PhNHNHPh is added last. If fast assembly of **2** occurs (pathway II), the color should change instantaneously to red-orange as **2** is formed, circumventing black **1a**. Otherwise, the normal pathway (I) will proceed, resulting in black intermediate **1a**, followed by formation of red **2**.

When this experiment is carried out in the presence of in situ-generated **1b**, the reaction proceeds straight to the pinned butterfly product, turning to red over the course of minutes (Scheme 4, pathway II). This is in contrast to the same reaction in the absence of **1b**, wherein the reaction turns quickly to black, and then slowly to red over the course of hours (Scheme 4, pathway I). The spectral evolution of this experiment is shown in Figure 3 (bottom), and demonstrates the direct appearance of **2**, circumventing **1a**.

While this competition kinetics experiment supports the plausibility of the fast assembly of **2** from **1b**, a more direct experiment was performed to associate the phenylamido ligands in **1b** to those in **2**. For this, a crossover labeling experiment was undertaken whereby the amide ligands of **1b** are labeled by the use of tolyl groups in place of phenyl. **1b-Tol** may be prepared in situ, or isolated as the product of $Mn(NR_2)_2$ + $TolNH_2$, a heteroleptic dimer, $Mn_2(\mu\text{-NHTol})_2(NR_2)_2(THF)_2$ (**1b-Tol**), which was identified by X-ray diffraction (XRD) (Figure 6). The overall geometry and bond metrics are similar to the previously characterized phenylamido dimer **1b**.

Formation of **1b-Tol** in situ from $Mn(NR_2)_2$ and toluidine, followed by addition of PhNHNHPh in pyridine solvent, results in the formation of a red solution very similar to that observed for compound **2-py**. Crystallographic analysis uncovers a new unit cell, however, suggesting a different compound. Structure solution and refinement identifies this

dx.doi.org/10.1021/ja508244x | J. Am. Chem. Soc. 2014, 136, 17974–17986

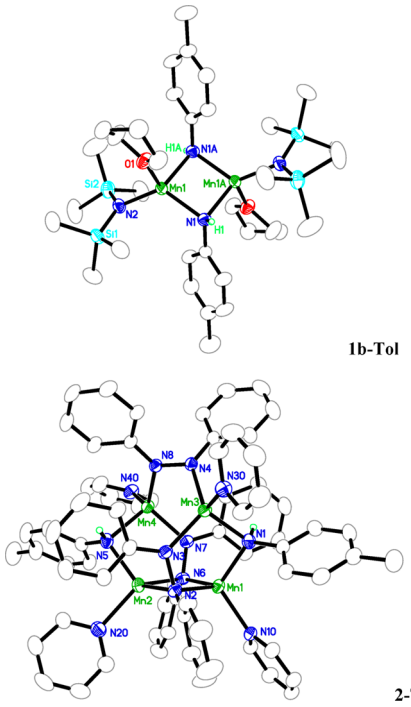

Figure 6. Thermal ellipsoid plots of $Mn_2(\mu\text{-NHTol})_2(NR_2)_2(THF)_2$ (**1b-Tol**) and $Mn_4(\mu_3\text{-PhN-NPh})_2(\mu\text{-PhN-NPh})(\mu\text{-NHTol})_2(py)_4{\cdot}py$ (**2-Tol**). Ellipsoids set at 50% probability level. Carbon atoms are shown as open ellipses. N−H hydrogen atoms shown as open circles. C−H hydrogens omitted for clarity. Pyridine lattice solvate in **2-Tol** is not shown.

cluster as the tolylamido analogue of **2** (**2-Tol**), containing exclusively tolylamido ligands and phenylhydrazido ligands with no evidence of compositional disorder (Figure 6). This material is obtained in ca. 90% yield. This experiment demonstrates that in the assembly of **2** from **1b**, the arylamido ligands of **1b** are maintained in the cluster assembly:

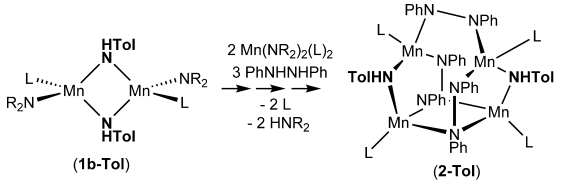

(11)

While this experiment does not rule out other assembly pathways, the speed, ease, and high yield from assembly of **2** from **1b** suggest it represents a dominant and low-barrier pathway. Furthermore, this approach has also been used to generate the all-tolyl version of the pinned butterfly cluster using *p*-toluidine and *p*-tolylhydrazine precursors (SI).

Crossover experiments involving mixtures of ditolyl- and diphenylhydrazine did not give crystalline products. Instead, a red glass resulted due to different crystal habits for the individual components of the mixture. This, along with the lack of useful NMR signatures, gives an inconclusive result for the crossover experiment, but due to the monodentate, weak-field nature of the amido ligands, extensive exchange between metal species is likely.

As an alternative means of tracing the migration of the bridging ligands of **1a** to **2**, we have examined the use of phenols in place of arylamines for this reaction. For instance, the phenoxide analogue of **1b** (**1b-OPh**) is synthesized in an analogous fashion and has already been reported with THF as a terminal ligand:[51]

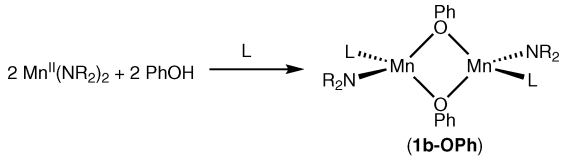

(12)

The assembly of **1c** with hydrazine and $Mn(NR_2)_2$ would then be expected to result in the O-labeled analogue of **2** (2-OAr):

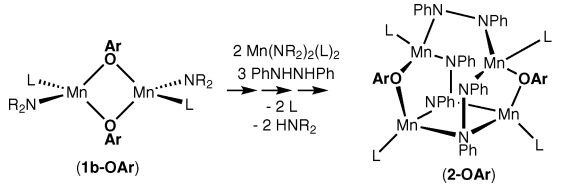

(13)

Unlike in the synthesis of **2-Tol**, the assembly of **2-OAr** does not proceed to the formation of pure, high yield product. Instead, the crystal structure is a compositionally disordered mixture of **2** and **2-OAr**. The structure shows strong evidence of the incorporation of oxygen atoms at the "amide" bridging positions, evidenced by the elongation of the ellipsoids of the O/N atoms and is better modeled as a compositional disorder between a pyramidal $PhNH^-$ ligand, and a planar PhO^- ligand (Figure 7). The details of the crystallography of this compositionally disordered crystal structure are discussed in greater detail in the Supporting Information.

The incomplete conversion of **1b-OAr** to **2-OAr** permitted the identification of another likely intermediate under these reaction conditions. In addition to the red **2-OAr** crystals, yellow $Mn_2(\mu\text{-OAr})_2(PhNNHPh)_2(py)_4$ (**1c-OPh**) is identified as a major component (Figure 7). This product represents the result of the protolysis of the silylamido ligands of **1b-OPh** by PhNHNHPh (see eq 12):

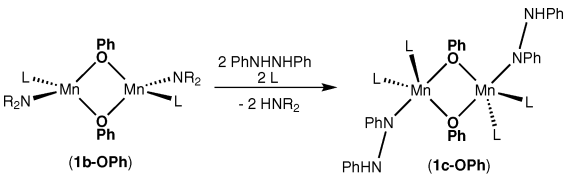

(14)

Due to the relief of steric strain by the protolysis of bulky NR_2^- ligands by the less sterically encumbered PhNNHPh, **1c** is five-coordinate, possessing four pyridine ligands. While this material is obtained only as a crystalline mixture along with **2-OPh**, we have also developed a synthetic protocol to obtain the tolyl analogue, $Mn_2(\mu\text{-OTol})_2(PhN\text{-}NHPh)_2(py)_2$ (**1c-OTol**) in pure form.

In addition to these O-substituted analogues, we have also prepared the μ-phenylamido-bridged **1c** using bipyridine as a terminal ligand (**1c-bpy**, Figure 7). The usage of bidentate bipyridine in place of pyridine results in five-coordinate manganese centers that are too sterically encumbered to proceed to the four-coordinate pinned butterfly cluster **2**, thus trapping the reaction at intermediate **1c**. Unlike **1c-OPh**, which has hydrazide ligands oriented in a *trans* configuration about a crystallographic inversion center, **1c-bpy** has hydrazide ligands in a cis configuration in the solid state, though in solution, ligands are likely exchanging, and both geometries probably

dx.doi.org/10.1021/ja508244x | J. Am. Chem. Soc. 2014, 136, 17974−17986

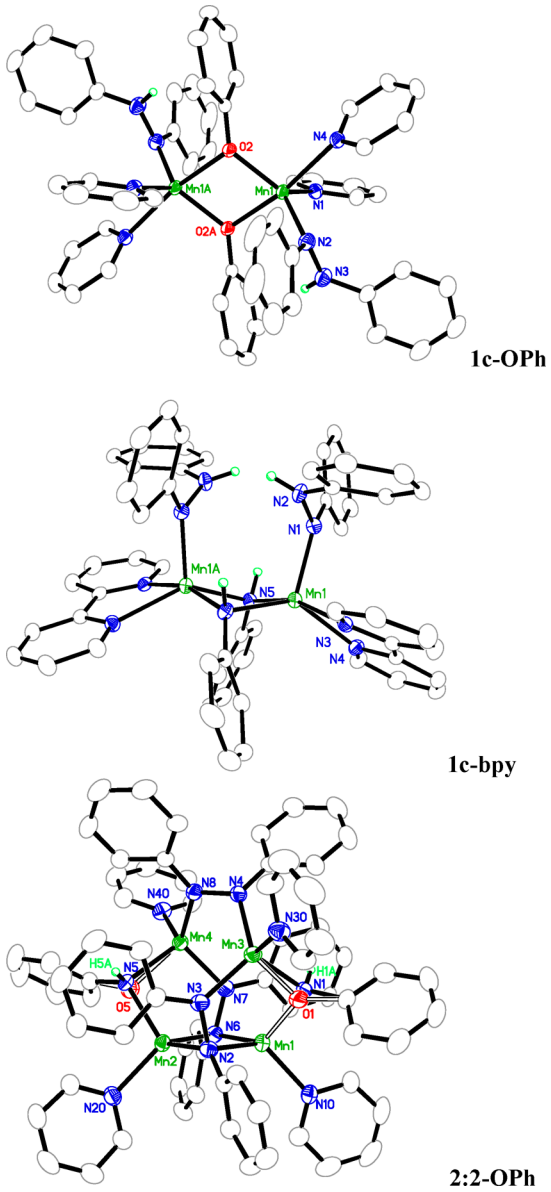

Figure 7. (Top) Thermal ellipsoid plot of $Mn_2(\mu\text{-OPh})_2$(PhN-NHPh)$_2$(py)$_4$ (**1c-OPh**), ellipsoids set at 50% probability level. (Middle) Thermal ellipsoid plot of $Mn_2(\mu\text{-NHPh})_2$(PhN-NHPh)$_2$-(bpy)$_2$ (**1c-bpy**) Ellipsoids set at 30% probability level. (Bottom) Thermal ellipsoid plot of compositionally disordered 0.30 $Mn_4(\mu_3\text{-}\eta_{1,2}$PhN-NPh$)_2(\mu\text{-}\eta_1$PhN-NPh$)(\mu\text{-OPh})_2(py)_4\cdot$0.70 $Mn_4(\mu_3\text{-}\eta_{1,2}$PhN-NPh$)_2(\mu\text{-}\eta_1$PhN-NPh$)(\mu\text{-NHPh})_2(py)_4$ (x**2-OPh**·y**2**). Thermal ellipsoids set at 50% probability level. N−H hydrogen atoms shown as open circles. Pyridine lattice solvate in **2-Tol** is not shown. C−H hydrogens omitted for clarity.

exist for both **1c-OPh** and **1c-bpy**. Attempts to isolate **1c** analogues with *N*-methyl-*N*,*N*′-diphenylhydrazine appear to proceed to a similar product based on the colorless solution and extrusion of 1 equiv of HNR_2, but have not yielded crystalline product.

Although we have not demonstrated the conversion of **1c** to final products, the isolation of the **1c** species as products of the incomplete formation of **2** is suggestive of **1c**'s possible role as an intermediate between the conversion of **1b** to **2**. The intermediacy of **1c**, whose formation from **1b** would require hydrazine, also explains why **1b** is isolated under limiting hydrazine conditions. The further reaction of **1c** with additional equivalents of PhNHNHPh and $Mn(NR_2)_2$ would result in completion of the conversion to **2**. Since the formation of **2** is incomplete, **1c** is isolated.

2.5. Summary. The above results may be integrated into an overall mechanistic scheme for the formation of **2** via the reaction of $Mn(NR_2)_2$ and PhNHNHPh, which is shown in Scheme 5. Reaction steps are lettered A−D, corresponding to sections 2.1−2.4, in which each is discussed (vide supra).

Scheme 5[a]

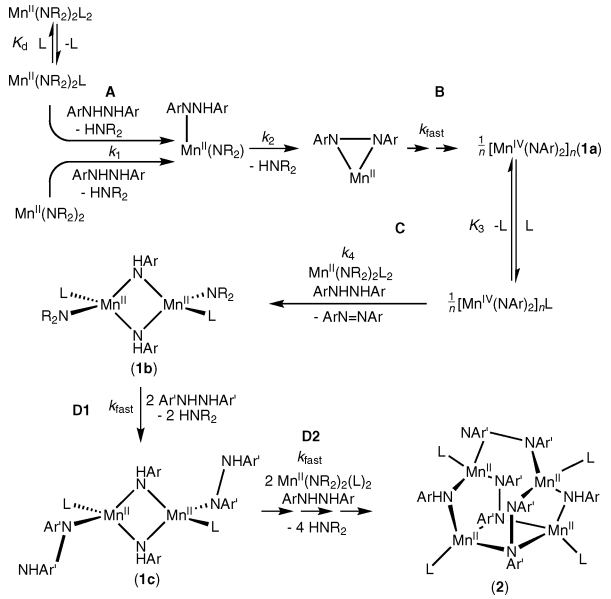

[a]Steps A−D correspond to text sections 2.1−2.4, respectively, in which each step is discussed.

The initial step of reaction A is solvent dissociation (unless the reaction is performed in non-ligating solvent) followed by the two-step protolytic replacement of bis(trimethysilyl)amido ligands by hydrazine to give a colorless Mn(II)-hydrazide intermediate drawn as a three membered metallacycle. While this geometry is not experimentally supported, it draws from the structural motifs of Mn-hydrazido complexes we have reported previously.[33] The dissociative ligand substitution is supported by solvent dependence of reaction kinetics. The initial protolysis step is supported by kinetic isotope effect, reactivity studies with methylated hydrazine (section 2.1), and by the fast appearance of N−H stretches of HNR_2 in the IR spectrum (Figure 4).

The Mn(II) hydrazide adduct reacts in step B, reductively cleaving the N−N bond (oxidative addition) to give a Mn(IV)-imido aggregate, which is supported by titration, colligative property measurements, and freeze-quench EPR studies (section 2.2). This intermediate is activated when solvent ligation disrupts the cluster core, and it abstracts hydrogen atoms (step C) from an additional equivalent of diarylhydrazine to produce azoarene and one or more Mn-amido intermediates (section 2.3), which assemble via multiple fast steps into compound **2** (steps D1 and D2). Compound **1b**, shown to be a precursor to **2** via competition kinetics and labeling experiments, would form first via the addition reaction of the Mn-phenylamido HAT product with an additional equivalent of $Mn(NR_2)_2$ (step C). In a limiting hydrazine environment, much of the reaction stops here, allowing the isolation of **1b**.

dx.doi.org/10.1021/ja508244x | J. Am. Chem. Soc. 2014, 136, 17974−17986

However, in the presence of sufficient ArNHNHAr, **1b** reacts further with hydrazine to give the terminally ligated hydrazide dimer **1c** (step D1). This dimer is isolated with bipyridine as a terminal ligand or as a phenyloxo analogue in the incomplete formation of **2** (section 2.4). Finally, protolytic addition reactions with further equivalents of $Mn(NR_2)_2$ and ArNHNHAr give the pinned butterfly cluster **2** (step D2). The source of the amide and hydrazide ligands are traced via labeling experiments using tolyl groups in place of phenyl groups or OPh groups in place of NHPh groups.

While the steps of the mechanism in Scheme 5 are well supported experimentally, it should be noted that there are other possible mechanisms by which **2** could assemble. Additionally, there are necessary additional rearrangement processes in the final (fast) stages of assembly, since the connectivity between the manganese atoms and the amide and hydrazide ligands changes drastically between **1c** and **2**. As self-assembly reactions are prone to be chaotic, and the weak-field, unchelated species discussed in this report are likely to be labile, numerous exchange reactions and rearrangement chemistries are possible. While it is not possible to unilaterally identify every possible intermediate in every possible assembly pathway in the formation of **2**, the mechanism shown in Scheme 5 is supported as a major (or perhaps *the* major) assembly pathway for **2**, and offers insights into fundamental assembly and rearrangement reactions at manganese cluster cores in the absence of geometry-directing ancillary chelating ligands.

3. CONCLUSION

Manganese cluster rearrangement reactions are an essential but unsolved part of the mechanism of water oxidation by the OEC. A renewed interest in manganese cluster model chemistry is evidenced by new reports of synthesis and reactions at novel Mn clusters. However, mechanistic scrutiny of reactions at Mn clusters is rarely seen, but will be an essential part of any attempt to understand biological water oxidation using model complexes. We have demonstrated here a pathway for assembly of a tetranuclear manganese pinned butterfly cluster supported by mechanistic studies. The approaches we are developing will pave the way for mechanistic interrogation of more biomimetic systems being developed in our laboratory.

4. EXPERIMENTAL SECTION

4.1. General. Compounds **1b**, **1b-OAr**, **1c-OAr**, **1c-bpy**, all variants of **2**, and $Mn[N(SiMe_3)_2]_2$ are highly air sensitive, decomposing with a vigorous exotherm and smoldering upon exposure to air. Thus, all operations were carried out under rigorous dry, anaerobic conditions using glovebox and Schlenk line techniques. All reagents were purchased and used as obtained from commercial providers (Aldrich, Fisher, Strem) unless otherwise specified. THF, pyridine, and HMDS were purified by distillation from sodium-benzophenone ketyl. Aniline was distilled using CaH_2. Dichloromethane (DCM), pentane, toluene, and benzene were purified using a PureSolv solvent purification system. Solvents were degassed and stored over 3 Å molecular sieves for 12 h before use. Deuterated NMR solvents were purchased from Sigma-Aldrich or Cambridge Isotope Laboratories, and stored over 3 Å molecular sieves for 12 h before use. ^{1}H NMR spectra were recorded on a Bruker Biospin 400 MHz spectrometer. Chemical shifts were referenced to the residual protiosolvent signal. Visible absorption spectra were acquired on a Shimadzu 2540 or 1800 spectrometer. Absorption spectroscopy was used to collect kinetic data using a Vernier Labquest data interface equipped with a Vernier colorimeter. Freezing point depression measurements were also performed using the Vernier labquest with a temperature probe. X-ray crystal structure determinations were performed using a Bruker Kappa APEX II DUO diffractometer equipped with an Oxford Cryostream. IR spectra were obtained using a Nicolet Magna 560 FTIR spectrometer with a liquid-N_2-cooled MCTA detector. Samples were analyzed in a liquid transmission cell. EPR spectra were recorded with a Bruker EMX spectrometer equipped with a Bruker ER 041 X G microwave bridge and a continuous-flow liquid helium cryostat (ESR900) coupled to an Oxford Instruments TC503 temperature controller. Spectra were obtained at 5 K under nonsaturating microwave power conditions (ν = 9.449 GHz, microwave power = 2.01 mW, modulation amplitude = 10 G, microwave frequency = 100 kHz, receiver gain = 5.02×10^3). Gas chromatography was performed on a Buck Scientific Model 910 gas chromatograph with a 15 m Restek MXT-1 column. He was used as a carrier gas. Kinetic simulations were performed using Simbiology in MATLAB R2013b. For simulation, fast steps (see Scheme 5) were set at 1000 M^{-1} s^{-1}. Initial values of all other rate constants, k_d, k_{-d}, k_1, k_2, k_3, k_{-3}, and k_4 were determined by fitting all these parameters to the kinetic data (vide infra) of the protio-hydrazine experiment. Then, k_d, k_{-d}, k_3, and k_{-3} were fixed at the resulting values, while k_1, k_2, and k_4 were fitted for both the protio and the deutero HAT experiments. CHN analyses were performed by Midwest Microlab or by the CENTC elemental analysis facility at the University of Rochester.

4.2. Synthesis. *N,N′*-Dimethyl-*N,N′*-diphenylhydrazine[52] and *N,N′*-diphenylhydrazine-d_2[43] (91% deuterated) were prepared by literature protocols. *N,N′*-Di-*p*-tolylhydrazine was prepared by a literature protocol[53] with the addition of air-exclusion techniques to avoid product decomposition in air.

$[Mn(NR_2)_2(THF)_2]$ and $[Mn(NR_2)_2]$ (R = $SiMe_3$). These compounds were prepared via a modification to literature protocol.[54] First, 20 g of $MnCl_2$ (125.8 g/mol, 159 mmol) was stirred in 250 mL of THF for 1 h in a nitrogen glovebox. Then 56 g of potassium bis(trimethylsilyl)-amide (199.3 g/mol, 281 mmol) dissolved in 200 mL of THF was slowly added over 20 min with constant stirring. The reaction mixture was allowed to stir for 2 h. The THF was then removed in vacuo at room temperature. Next, 500 mL of pentane was used to dissolve the $Mn(NR_2)_2(THF)_2$, and the KCl was removed by filtration using a coarse frit. The solution was concentrated to 200 mL and stored overnight at −30 °C. Approximately 25 g of $Mn(NR_2)_2(THF)_2$ (48.1 mmol, 34.4% yield) was isolated. Unit cell (XRD): monoclinic *P*, a = 13.8679(19) Å, b = 12.1188(16) Å, c = 18.512(3) Å, β = 97.116(2)°.

$Mn[N(SiMe_3)_2]_2$. This compound was prepared by distillation of $Mn(NR_2)_2(THF)_2$ at 110 °C under dynamic vacuum. Product was collected in a 250 mL Schlenk flask, dissolved in pentane, and crystallized at −30 °C, yielding 13.9 g (36.9 mmol, 76.7% yield). Unit cell (XRD): monoclinic *C*, a = 18.031(13) Å, b = 14.955(11) Å, c = 18.693(14) Å, β = 121.21(2)°.

$[Mn(NHPh)_2]_n$. Method A: To a solution of $Mn(NR_2)_2(THF)_2$ (R = $SiMe_3$) (147 mg, 0.2827 mmol) in 2.5 mL of pyridine was added a solution of NH_2Ph (53 μL, 0.5814 mmol) in 2.5 mL of pyridine. The mixture was allowed to react overnight and resulted in a yellow suspension. The precipitate was allowed to settle, and the solution was decanted. The solid was dried in vacuo, and a powder diffraction pattern was collected at 100 K.

Method B: To a solution of $Mn(NR_2)_2$ (R = $SiMe_3$) (225 mg, 0.5989 mmol) in 2 mL of benzene was added a solution of PhNHNHPh (110 mg, 0.5978 mmol) in 2 mL of benzene. The resulting black solution was allowed to react for 10 min before the addition of another solution of PhNHNHPh (110 mg, 0.5978 mmol) in 10 mL of THF. Over the course of 15−20 min, the black solution changed to a red color. The solution was allowed to react overnight. This solution was dried in vacuo, and the solid residue was extracted with pentane. The remaining solid was extracted with pyridine and resulted in a red solution with a yellow suspension. The yellow solid was allowed to settle, and the red solution was decanted. The solid was dried in vacuo, and a powder diffraction pattern was collected at 100 K.

*$Mn(\mu\text{-}NHPh)_2[N(SiMe_3)_2]_2(THF)_2$ (**1b**).* Compound **1b** was prepared as previously described.[26] Alternatively, **1b** was prepared via reaction of $Mn[N(SiMe_3)_2]_2$ with crude $[Mn(NHPh)_2]_n$. To 135 mg of $Mn(NR_2)_2(THF)_2$ (0.2596 mmol) in 1.5 mL of pyridine was added 50

dx.doi.org/10.1021/ja508244x | J. Am. Chem. Soc. 2014, 136, 17974−17986

μL of NH_2Ph (0.5485 mmol) in 1.5 mL of pyridine. This solution was allowed to react for 30 min. During the reaction time, the yellow solution precipitated and formed a yellow powder. To this suspension was added an additional 135 mg of $Mn(NR_2)_2(THF)_2$ (0.2596 mmol) in 2 mL of pyridine. The resulting solution was allowed to react overnight at room temperature. After that time, the solution was placed in a freezer at −40 °C. Over the course of 2 weeks, the yellow powder settled, and pink crystals began to form. The suspension was decanted, and the crystals were rinsed with ∼3 mL of pentane three times. The crystals were identified using X-ray crystallography and dried in vacuo. A total of 36 mg of pink crystals of **1b** (0.04675 mmol, 18% yield) was isolated. Unit cell (XRD): monoclinic *P*, a = 8.817(4) Å, b = 21.151(9) Å, c = 10.788(4) Å, β = 95.286(7)°, volume = 2003.3(14) Å^3.

*$[Mn_2(\mu\text{-NH-p-Tol})_2(NR_2)_2(THF)_2]$ (**1b-Tol**, R = $SiMe_3$).* **1b-Tol** was prepared on the basis of a previously reported protocol.[26] To $Mn[NR_2]_2$ (142 mg, 0.378 mmol) in *n*-pentane (10 mL) was added *p*-toluidine (46 mg, 0.430 mmol) in THF (5 mL). After 8 h at room temperature in a sealed vial, pink crystals precipitated. The resulting light pink crystals were isolated by decanting and rinsed with pentane. A total of 113 mg of pink crystals (0.177 mmol, 93.8% yield) was isolated and dried under vacuum. Unit cell (XRD): triclinic *P*, a = 11.1968(16) Å, b = 11.5552(16) Å, c = 17.838(3) Å, α = 89.739(3)°, β = 86.275(3)°, γ = 77.148(2)°.

*$[Mn_4(\mu_3\text{-}N_2Ph_2)_2(\mu\text{-}N_2Ph_2)(\mu\text{-PhNH})_2(py)_4]$ (**2-py**).* **2-py** was prepared on the basis of a previously reported synthesis[26] or the following improved protocol using aniline and diphenylhydrazine as ligand sources, which gives better purity than using diphenylhydrazine alone. To a solution of $Mn[N(Si(CH_3)_3)_2]_2$ (210 mg, 0.559 mmol) in 1 mL of pyridine and 5 mL of pentane was added a solution of aniline (30 μL, 0.315 mmol) in 3 mL of pyridine, immediately followed by a solution of PhNHNHPh (85 mg 0.462 mmol) in 4 mL of toluene. This resulted in a color change from yellow to orange to red-amber over the course of 1 min. Over the course of 3 h at room temperature, red crystalline material precipitated. The solid was isolated by decanting and rinsed with 3 mL of pentane three times. A total of 162 mg of red needles (0.128 mmol, 77% yield) was isolated and dried under vacuum. Anal. Calcd for $C_{68}H_{62}Mn_4N_{12}$: C, 64.44; H, 4.93; N, 13.27. Found: C, 64.74, H, 5.18; N, 13.13. Unit cell (XRD): monoclinic *P*, a = 16.516 Å, b = 15.842(4) Å, c = 16.591(5) Å, β = 116.311(4)°, or monoclinic P, a = 22.764(3) Å, b = 14.0803(16) Å, c = 24.148(3) Å, β = 109.392(2)°.

*$[Mn_4(\mu_3\text{-}N_2Ph_2)_2(\mu\text{-}N_2Ph_2)(\mu\text{-NH-p-Tol})_2(py)_4]$ (**2-Tol**).* **2-Tol** was prepared using the same protocol as for **2-py** above, except for the use of *p*-toluidine in place of aniline, using the following amounts: $Mn[N(Si(CH_3)_3)_2]_2$ (161 mg, 0.429 mmol), toluidine (25 mg, 0.234 mmol), PhNHNHPh (80 mg, 0.435 mmol). A total of 161 mg of red needles was isolated and dried under vacuum (124.1 μmol, 91.8% yield). Anal. Calcd for $C_{70}H_{66}Mn_4N_{12}$: C, 64.80; H, 5.29; N, 12.96. Found: C, 64.87, H, 5.14; N, 13.10. Unit cell (XRD): monoclinic *P*, a = 14.7510(10) Å, b = 24.8219(16) Å, c = 19.4882(14) Å, β = 92.7590(10)°, or monoclinic *P*, a = 16.7834(16) Å, b = 15.7756(15) Å, c = 17.4353(16) Å, β = 117.807(3)°.

$[Mn_4(\mu_3\text{-}N_2Tol_2)_2(\mu\text{-}N_2Tol_2)(\mu\text{-NH-p-Tol})_2(py)_4]$. This compound was prepared using the same protocol as for **2-py** and **2-Tol** above, except for the use of *N*,*N*′-di-*p*-tolylhydrazine in place of PhNHNHPh and *p*-toluidine in place of aniline, using the following amounts: $Mn[N(Si(CH_3)_3)_2]_2$ (161 mg, 0.429 mmol), toluidine (25 mg, 0.234 mmol), ditolylhydrazine (80 mg, 0.435 mmol). A total of 100 mg of red needles was isolated and dried under vacuum (72.5 μmol, 67.7% yield). Anal. Calcd for $C_{76}H_{86}Mn_4N_{12}$: C, 65.779; H, 6.251; N, 12.120. Found: C, 66.067; H, 6.651; N, 11.662. Unit cell (XRD): monoclinic *C*, a = 19.981(2) Å, b = 16.5186(16) Å, c = 22.047(2) Å, β = 109.417°.

*$x[Mn_4(\mu_3\text{-}N_2Ph_2)_2(\mu\text{-}N_2Ph_2)(\mu\text{-PhO})_2(py)_4]\cdot(1-x)[Mn_4(\mu_3\text{-}N_2Ph_2)_2(\mu\text{-}N_2Ph_2)(\mu\text{-NHPh})_2(py)_4]$ (**x2-OPh·(1−x)2-py**, $x \approx 0.25-0.3$) and $[Mn_2(\mu\text{-OPh})_2(PhNNHPh)_2(py)_4]$ (**1c-OPh**).* To a solution of $Mn[N(Si(CH_3)_3)_2]_2$ (220 mg, 0.586 mmol) in 1 mL of pyridine and 5 mL of pentane was added a solution of phenol (23 mg, 0.245 mmol) in 5 mL of DCM, immediately followed by a solution of PhNHNHPh (65 mg, 0.353 mmol) in 4 mL of DCM. This resulted in a color change from yellow to orange to red-amber over the course of 1 min. Over the course of 3 h at room temperature, a mixture of red and yellow crystalline material precipitated, which was isolated by decanting and rinsing with pentane. Crystal structures of the red material showed a mixture of $x[Mn_4(\mu_3\text{-}N_2Ph_2)_2(\mu\text{-}N_2Ph_2)(\mu\text{-PhO})_2(py)_4]$ and $(1-x)[Mn_4(\mu_3\text{-}N_2Ph_2)_2(\mu\text{-}N_2Ph_2)(\mu\text{-PhNH})_2(py)_4]$, with x between 25 and 30 mol % oxygen labeling. Crystal structures of the yellow material identified it as $[Mn_2(\mu\text{-OPh})_2(PhNNHPh)_2(py)_4]$ (**1c-OPh**). Unit cell (XRD): monoclinic *C*, a = 12.703(3) Å, b = 13.905(4) Å, c = 13.986(4) Å, β = 97.690(5)°.

*$[Mn_2(\mu\text{-p-OTol})_2(NR_2)_2(THF)_2]$ (**1b-OTol**).* To $Mn[N(SiMe_3)_2]_2(THF)_2$ (317 mg, 0.6096 mmol) in 5 mL of THF was added cresol (66 mg, 0.6096 mmol) in 5 mL of THF. The solution was stirred and heated in a pressure flask at ∼65 °C for 2 h. After the solution was allowed to cool, it was concentrated to 3 mL and placed in the freezer at −40 °C for 2 days. Light pink crystals were formed, and the solution was decanted. The crystals were rinsed three times with ∼5 mL of pentane and dried under vacuum. Yield: 107 mg (0.1356 mmol, 44.6%). Anal. Calcd for $C_{34}H_{66}Mn_2N_2O_4Si_4$: C, 51.758; H, 8.438; N, 3.553. Found: C, 52.019; H, 8.318; N, 3.405. Unit cell (XRD): monoclinic *P*, a = 8.8333(17) Å, b = 17.029(3) Å, c = 14.282(3) Å, β = 93.673(4)°.

*$[Mn_2(\mu\text{-p-OTol})_2(PhNNHPh)_2(Pyr)_4]$ (**1c-OTol**).* To $[Mn_2(\mu\text{-p-OTol})_2(NR_2)_2(THF)_2]$ (107 mg, 0.1356 mmol) in 2 mL of pyridine was added PhNHNHPh (50 mg, 0.2717 mmol) in 2 mL of pyridine. The solution was allowed to react for 10 min and was concentrated to 2 mL. A vapor diffusion recrystallization was prepared in a double-vial apparatus with ether as precipitant and placed in a freezer at −40 °C for 2 days. Yellow crystals were formed and identified with X-ray diffractometry. The solution was decanted, and the crystals were rinsed three times with ∼5 mL of pentane and dried under vacuum. Yield: 42 mg (0.0417 mmol, 30.7%). UV−vis (THF): λ_{max} [nm] ($\varepsilon \times 10^{-3}$) 245 (150), 290 (35), 335 (6.6). Anal. Calcd for $C_{53}H_{51}Mn_2N_7O_2$ (loss of one pyridine): C, 68.587; H, 5.543; N, 10.571. Found: C, 68.467; H, 5.466; N, 10.822. Unit cell (XRD): monoclinic *P*, a = 12.6250(9) Å, b = 15.0713(10) Å, c = 13.5101(9) Å, β = 98.2840(10)°.

$[Mn(NR_2)_2(bpy)]$. To a solution of $Mn[N(SiMe_3)_2]_2(THF)_2$ (236 mg, 0.4538 mmol) in 5 mL of pentane was added a solution of 2,2′-bipyridine (65 mg, 0.4162 mmol) in 1 mL of ether. The solutions were mixed and immediately changed to a red color. The solution was placed in a freezer at −40 °C for 4 h. Red needles were formed, and the resulting solution was decanted. The red needles were identified with XRD. The red needles were rinsed three times with ∼5 mL of cold pentane and dried under vacuum. Yield: 170 mg (0.3195 mmol, 76.9%). Anal. Calcd for $C_{56}H_{50}Mn_2N_{10}$: C, 69.115; H, 5.183; N, 14.402. Found: C, 68.766; H, 5.149; N, 13.951. Unit cell (XRD): monoclinic *C*, a = 15.1502(19) Å, b = 28.231(4) Å, c = 8.2921(10) Å, β = 106.295(3)°.

*$[Mn_2(\mu\text{-NHPh})_2(HN_2Ph_2)_2(bpy)_2]$ (**1c-bpy**).* To a solution of $[Mn(NR_2)_2(Bpy)]$ (R = $SiMe_3$) (220 mg, 0.4231 mmol) in 2 mL of ether was added a solution of PhNHNHPh (120 mg, 0.6522 mmol) in 3 mL of toluene. The resulting solution was allowed to react at room temperature for 16 h. Dark red crystals were formed, and the solution was decanted. The crystals were identified with XRD, rinsed three times with ∼5 mL of pentane, and dried under vacuum. Yield: 146 mg (0.1502 mmol, 70.9%). UV−vis (DCM): λ_{max} [nm] ($\varepsilon \times 10^{-3}$) 384 (45), 330 (18). Anal. Calcd for $C_{34}H_{66}Mn_2N_2O_4Si_4$: C, 51.758; H, 8.438; N, 3.553. Found: C, 52.019; H, 8.318; N, 3.405. Unit cell (XRD): monoclinic *C*, a = 26.474(7) Å, b = 10.909(3) Å, c = 20.872(9) Å, β = 127.903(5)°.

4.3. X-ray Crystallography. Single crystals were obtained directly from the reaction mixtures in all cases. Crystals were suspended in Paratone-N oil or Apiezon-N grease, mounted on a MiTeGen loop, and cooled in the cryostream. Data were collected using Mo Kα radiation in phi/omega scans using COSMO (Bruker AXS). Integration was performed with SAINT (Bruker AXS), and scaling and absorption corrections were applied using SADABS (Bruker AXS). Space group determination was performed using X-PREP (Bruker AXS). Structure solution and refinement was performed using

the SHELXTL package (Sheldrick). Crystallographic data tables were generated using the APEX2 software suite (Bruker AXS).

4.4. Difference Fourier Transform Infrared (FTIR) Spectroscopy. Stock solutions were a 25 mL solution of $Mn[N(SiMe_3)_2]_2$ (1146 mg, 3.05 mmol, 122 mM) in pyridine, and a 10 mL solution of PhNHNHPh (300 mg, 1.64 mmol, 164 mM) in pyridine; 1 mL aliquots of each were mixed into a 5 mL vial and shaken. This reaction mixture was immediately injected into a NaCl fixed cell and placed in a Nicolet Magna 560 FTIR spectrometer with a liquid-N_2-cooled MCTA detector. Scans were collected over 7 h. Due to overlap with other signals, the hexamethyldisilazane N−H stretch was plotted in Figure 4 as the absorbance at it is peak (3370 cm^{-1}) minus the absorbance at the valley (3425 cm^{-1}).

4.5. Electron Paramagnetic Resonance (EPR) Spectroscopy. (Figure S8 bottom) All samples were prepared in a glovebox, transferred to EPR tubes, and stored in a bath of liquid nitrogen for several hours during transport to Johns Hopkins for analysis.

*In Situ Spectrum of **1a**.* The sample was prepared by dissolving 61 mg of $Mn[N(Si(CH_3)_3)_2]_2$ in 10 mL of toluene. A 6 mL portion of this solution was mixed with 17 mg of PhNHNHPh dissolved in 5 mL of toluene; the remaining 4 mL was mixed with 12 mg of PhNHNHPh dissolved in 2 mL of THF.

*Spectrum of **1a** and **1a**$^-$ in Toluene.* An approximately 0.36 M solution of sodium benzophenone ketyl radical was prepared by the dissolution of 658 mg of benzophenone in 10 mL of diethyl ether. To this was added a solid chunk of sodium (∼1g) sliced into small pieces using a spatula. This was stored for 24 at room temperature.

A 65 mg sample of $Mn[N(Si(CH_3)_3)_2]_2$ (THF-free) was dissolved in 10 mL of toluene (0.173 mmol). A 5 mL portion of this solution was mixed with 14 mg of PhNHNHPh dissolved in 5 mL of toluene (0.076 mmol).

An identical sample was prepared except that a substoichiometric amount (approximately 50 μL) of the 0.36 M sodium benzophenone ketyl radical solution in diethyl ether (0.018 mmol) was added.

4.6. Kinetic Studies. Solutions of 47.3 mM $Mn[N(Si(CH_3)_3)_2]_2$ and 96.7 mM PhNHNHPh were prepared in 5 mL volumetric flasks using THF as the solvent; 1.2 mL aliquots of each were then mixed and placed in a Spectrocell quartz cuvette with a 1 cm path length. A Vernier LabQuest sensor interface equipped with a colorimeter was used to collect scans every 3 s over 3 h at 635 nm to monitor the appearance and disappearance of the dark intermediate. This experiment was repeated using 52.1 mM $Mn[N(Si(CH_3)_3)_2]_2$ with 85.3 mM 1,2-dimethyl-1,2-diphenylhydrazine (no reaction observed), and 45.7 mM $Mn[N(Si(CH_3)_3)_2]_2$ with 96.8 mM *N*,*N*′-diphenylhydrazine-d_2. See Figure 3 for data.

*Monitoring Formation of **2** from **1b**, $Mn[N(SiMe_3)_2]_2$, and PhNHNHPh.* In order to test the notion that the formation of **2** from the above reagents was fast, a colorimetric experiment was performed analogous to the kinetic experiments discussed in the preceding paragraph, but with **1b** already pre-formed in situ. A solution of 88 mg of $Mn(NR_2)_2$ (R = $SiMe_3$) (0.2342 mmol) and 12 μL of NH_2Ph (0.1316 mmol) was prepared in a 5 mL volumetric flask using THF. A 5 mL solution of 36 mg of PhNHNHPh (0.1957 mmol) in THF was added to this solution and mixed. A 3 mL portion of the resulting solution was placed into a 1 cm path length quartz cuvette. The cuvette was placed into a UV−vis spectrometer, and scans were collected. Settings for collection: 2 nm intervals, fast collection speed, 0 s time intervals. See Figure 3 for data.

4.7. HAT from Dihydroanthracene. First, 572 mg of $Mn(NR_2)_2(THF)_2$ in 2 mL of pyridine and 4 mL of THF was mixed with 390 mg of DHA in 5 mL of THF. To this solution was added 275 mg of PhNHNHPh dissolved in 4 mL of THF and 3 mL of toluene. After 30 min, the solution was dried completely. This solution was analyzed by gas chromatography (GC) and ^{1}H NMR. For GC analysis, a 25 mg sample was dissolved in 5 mL of benzene with 17 mg of napthalene, exposed to air, and filtered. A scraping of the solid was dissolved in benzene-d_6 for ^{1}H NMR analysis.

A separate reaction was carried out in the absence of ligating THF by adding 380 mg of DHA dissolved in 5 mL of benzene to 490 mg of $Mn(NR_2)_2$ dissolved in 5 mL of benzene. To this was added 275 mg of PhNHNHPh dissolved in 4 mL of benzene. After 30 min, the resulting black solution was dried by vacuum. For GC analysis, a 26 mg sample was dissolved in 5 mL of benzene with 18 mg of napthalene, exposed to air, and filtered. A scraping of the solid was dissolved in benzene-d_6 for NMR analysis.

Solutions were analyzed by GC and ^{1}H NMR for comparison with standard solutions of naphthalene, anthracene, DHA, and azobenzene. The reaction in ligating solvent (THF) resulted in a stochiometric production of anthracene (1 anthracene:4 Mn), while the reaction in non-ligating solvent resulted in no anthracene production.

4.8. Determination of Stoichiometry of Formation of 1a. A solution of $Mn[N(SiMe_3)_2]_2$ (73 mg, 0.1943 mmol) was prepared in benzene using a 20 mL volumetric flask (9.7 mM). A second solution of PhNHNHPh (36 mg, 0.1957 mmol) was prepared in benzene using a 10 mL volumetric flask (19.6 mM). To separate 10 mL volumetric flasks were added 1 mL of $Mn[N(SiMe_3)_2]_2$ solution and varying amounts of the PhNHNHPh solution (250, 300, 335, 400, 500, 600, 670, 750, and 1000 μL). The resulting solutions were then diluted to 10 mL using benzene, placed in 1 cm quartz cuvettes, and immediately analyzed by UV−vis absorption spectroscopy from 290 to 800 nm.

4.9. Hexamethyldisilazane Quantification from Formation of 1a. To a solution of $Mn(NR_2)_2$ (R = $SiMe_3$) (83 mg, 0.2209 mmol) in 1 mL of C_6D_6 was added a solution of PhNHNHPh (49 mg, 0.2663 mmol) in 1 mL of C_6D_6. The resulting black solution was spiked with 0.383 g of DCM, and the ^{1}H NMR spectrum was recorded. A total of 61 mg of HMDS was quantified by ^{1}H NMR (0.3780 mmol, 85.9% yield).

4.10. Azoarene Quantification from Re-initiation of HAT Reaction by Addition of THF to 1a. *Azobenzene.* To a solution of $Mn(NR_2)_2$ (R = $SiMe_3$) (225 mg, 0.5989 mmol) in 2 mL of benzene was added a solution of PhNHNHPh (110 mg, 0.5978 mmol) in 2 mL of benzene. The resulting black solution was allowed to react for 10 min before the addition of another solution of PhNHNHPh (110 mg, 0.5978 mmol) in 10 mL of THF. Over the course of 15−20 min, the black solution changed to a red color. The solution was allowed to react for 16 h. This solution was dried in vacuo, and the solid residue was extracted with pentane. The pentane extract was dried and dissolved in ∼2 mL of C_6D_6. The solution was then spiked with 15 μL of THF, and the ^{1}H NMR spectrum was recorded. A total of 106 mg of azobenzene was quantified by ^{1}H NMR (0.5824 mmol, 97.2% yield).

Azotoluene. To a solution of $Mn(NR_2)_2$ (R = $SiMe_3$) (249 mg, 0.6627 mmol) in 2 mL of benzene was added a solution of PhNHNHPh (122 mg, 0.6630 mmol) in 2 mL of benzene. The resulting black solution was allowed to react for 10 min before the addition of another solution of *N*,*N*′-ditolylhydrazine (140 mg, 0.6604 mmol) in 10 mL of THF. A significant color change was not observed immediately, and the solution was allowed to stir for 16 h. This solution was dried in vacuo, and the solid residue was extracted with pentane. The pentane extract was dried and dissolved in ∼2 mL of C_6D_6. The solution was then spiked with 15 μL of THF, and the ^{1}H NMR spectrum was recorded. A total of 88 mg of azotoluene was quantified by ^{1}H NMR (0.4190 mmol, 63.3% yield).

4.11. Freezing Point Depression by 1a. *Preparation of Standard Solutions.* For each measurement, ∼3 mL of each solution was placed in a small vial which was then capped with a septum. A temperature probe was inserted into the septum, and the apparatus was placed in a freezer at −40 °C. One measurement was taken per second, and each trial lasted between 20 and 30 min. The freezing point was calculated from the plateau of the cooling curves.

To generate a calibration curve for freezing point depression, azobenzene was used as a standard. As all in situ preparations of **1a** contain predictable amounts of HMDS byproduct, this compound was also included in the calibration curve. Several benzene, HMDS, and azobenzene standards were prepared with varying amounts of azobenzene. The HMDS:azobenzene concentration ratios were 1:1, 2:1, 3:1, 4:1, and 8:1. The respective masses are as follow (benzene, HMDS, azobenzene, all in grams), according to mole ratios: 2.764, 0.342,0.388; 2.791,0.335,0.194; 2.750,0.330,0.129; 2.728,0.325,0.097; and 2.729,0.322,0.049. Another standard was prepared with no

azobenzene, 2.808 g of benzene, and 0.345 g of HMDS, and one standard of pure benzene was used as well.

Freezing Point Depression of in Situ Solution of ***1a****.* To 400 mg of MnBis (1.065 mmol) in 1.345 g of benzene was added 196 mg of PhNHNHPh (1.065 mmol) in 1.350 g of benzene. The freezing point of this solution was determined.

■ ASSOCIATED CONTENT

Ⓢ Supporting Information

Crystallographic tables and crystallographic information files (CIF), additional discussion of compositional disorder of **2-OPh**, details of testing and rejection of the silylamine autocatalysis mechanism, ^{1}H NMR spectra and GC traces of DHA-HAT experiments, solvent-dependent kinetic experiments, details of kinetic simulation model, determination of the stoichiometry of formation of **1a**, and in situ EPR spectra, freezing point depression data, and powder patterns of $[Mn(NHPh)_2]_n$. This material is available free of charge via the Internet at http://pubs.acs.org.

■ AUTHOR INFORMATION

Corresponding Author

mzdilla@temple.edu

Present Addresses

[†]R.A.B.: Department of Chemistry, The Johns Hopkins University, Baltimore, MD 21218

[‡]S.F.M.: Department of Chemistry, Yale University, New Haven, CT 06520

Author Contributions

[§]C.R.H. and M.R.G. contributed equally to this work.

Notes

The authors declare no competing financial interest.

■ ACKNOWLEDGMENTS

Support of this research by the National Science foundation through grant 1254545, and by the Office of Naval Research through grant N00014-13-1-0539, is gratefully acknowledged. Prof. David P. Goldberg of Johns Hopkins University is gratefully acknowledged for assistance with EPR measurements. We thank Andro-Marc Pierre Louis and Prof. Daniel R. Strongin of Temple University for assistance with FTIR measurements.

■ REFERENCES

(1) Yano, J.; Yachandra, V. *Chem. Rev.* **2014**, *114*, 4175.

(2) Najafpour, M. M.; Moghaddam, A. N.; Allakhverdiev, S. I.; Govindjee. *BBA-Bioenergetics* **2012**, *1817*, 1110.

(3) Dau, H.; Zaharieva, I.; Haumann, M. *Curr. Opin. Chem. Biol.* **2012**, *16*, 3.

(4) Rivalta, I.; Brudvig, G. W.; Batista, V. S. *Curr. Opin. Chem. Biol.* **2012**, *16*, 11.

(5) Yamanaka, S.; Kanda, K.; Saito, T.; Umena, Y.; Kawakami, K.; Shen, J. R.; Kamiya, N.; Okumura, M.; Nakamura, H.; Yamaguchi, K. In *Advances in Quantum Chemistry*; John, R. S., Erkki, J. B., Eds.; Academic Press: Kidlington, Oxford, UK, 2012; Vol. *64*, p 121.

(6) Grundmeier, A.; Dau, H. *BBA-Bioenergetics* **2012**, *1817*, 88.

(7) Umena, Y.; Kawakami, K.; Shen, J.-R.; Kamiya, N. *Nature* **2011**, *473*, 55.

(8) Mayer, J.; Rhile, I.; Larsen, F.; Mader, E.; Markle, T.; Dipasquale, A. *Photosynth. Res.* **2006**, *87*, 21.

(9) Radmer, R.; Kok, B. *Annu. Rev. Biochem.* **1975**, *44*, 409.

(10) Yachandra, V. K.; Sauer, K.; Klein, M. P. *Chem. Rev.* **1996**, *96*, 2927.

(11) Siegbahn, P. E. M. *Chem.—Eur. J.* **2008**, *14*, 8290.

(12) Sproviero, E. M.; McEvoy, J. P.; Gascón, J. A.; Brudvig, G. W.; Batista, V. S. *Photosynth. Res.* **2008**, *97*, 91.

(13) Gatt, P.; Stranger, R.; Pace, R. J. *J. Photochem. Photobiol.* **2011**, *104*, 80.

(14) Kupitz, C.; Basu, S.; Grotjohann, I.; Fromme, R.; Zatsepin, N. A.; Rendek, K. N.; Hunter, M. S.; Shoeman, R. L.; White, T. A.; Wang, D.; James, D.; Yang, J.-H.; Cobb, D. E.; Reeder, B.; Sierra, R. G.; Liu, H.; Barty, A.; Aquila, A. L.; Deponte, D.; Kirian, R. A.; Bari, S.; Bergkamp, J. J.; Beyerlein, K. R.; Bogan, M. J.; Caleman, C.; Chao, T.-C.; Conrad, C. E.; Davis, K. M.; Fleckenstein, H.; Galli, L.; Hau-Riege, S. P.; Kassemeyer, S.; Laksmono, H.; Liang, M.; Lomb, L.; Marchesini, S.; Martin, A. V.; Messerschmidt, M.; Milathianaki, D.; Nass, K.; Ros, A.; Roy-Chowdhury, S.; Schmidt, K.; Seibert, M.; Steinbrener, J.; Stellato, F.; Yan, L.; Yoon, C.; Moore, T. A.; Moore, A. L.; Pushkar, Y.; Williams, G. J.; Boutet, S.; Doak, R. B.; Weierstall, U.; Frank, M.; Chapman, H. N.; Spence, J. C. H.; Fromme, P. *Nature* **2014**, *513*, 261.

(15) Kanady, J. S.; Tsui, E. Y.; Day, M. W.; Agapie, T. *Science* **2011**, *333*, 733.

(16) Mukherjee, S.; Stull, J. A.; Yano, J.; Stamatatos, T. C.; Pringouri, K.; Stich, T. A.; Abboud, K. A.; Britt, R. D.; Yachandra, V. K.; Christou, G. *Proc. Natl. Acad. Sci. U.S.A.* **2012**, *109*, 2257.

(17) Mukhopadhyay, S.; Mandal, S. K.; Bhaduri, S.; Armstrong, W. H. *Chem. Rev.* **2004**, *104*, 3981.

(18) Fout, A. R.; Zhao, Q.; Xiao, D. J.; Betley, T. A. *J. Am. Chem. Soc.* **2011**, *133*, 16750.

(19) Kanady, J. S.; Mendoza-Cortes, J. L.; Tsui, E. Y.; Nielsen, R. J.; Goddard, W. A.; Agapie, T. *J. Am. Chem. Soc.* **2012**, *135*, 1073.

(20) Mukhopadhyay, S.; Mok, H. J.; Staples, R. J.; Armstrong, W. H. *J. Am. Chem. Soc.* **2004**, *126*, 9202.

(21) Wang, S.; Tsai, H.-L.; Hagen, K. S.; Hendrickson, D. N.; Christou, G. *J. Am. Chem. Soc.* **1994**, *116*, 8376.

(22) Yagi, M.; Wolf, K. V.; Baesjou, P. J.; Bernasek, S. L.; Dismukes, G. C. *Angew. Chem., Int. Ed.* **2001**, *40*, 2925.

(23) Limburg, J.; Vrettos, J. S.; Liable-Sands, L. M.; Rheingold, A. L.; Crabtree, R. H.; Brudvig, G. W. *Science* **1999**, *283*, 1524.

(24) Taguchi, T.; Stone, K. L.; Gupta, R.; Kaiser-Lassalle, B.; Yano, J.; Hendrich, M. P.; Borovik, A. S. *Chem. Sci.* **2014**, *5*, 3064.

(25) Berlinguette, C. P.; Holm, R. H. *J. Am. Chem. Soc.* **2006**, *128*, 11993.

(26) Hamilton, C. R.; Baglia, R. A.; Gordon, A. D.; Zdilla, M. J. *J. Am. Chem. Soc.* **2011**, *133*, 4208.

(27) Olmstead, M. M.; Power, P. P.; Shoner, S. C. *Inorg. Chem.* **1991**, *30*, 2547.

(28) Cen, W.; MacDonnell, F. M.; Scott, M. J.; Holm, R. H. *Inorg. Chem.* **1994**, *33*, 5809.

(29) Sharp, C. R.; Duncan, J. S.; Lee, S. C. *Inorg. Chem.* **2010**, *49*, 6697.

(30) Cleland, W. E.; Holtman, D. A.; Sabat, M.; Ibers, J. A.; DeFotis, G. C.; Averill, B. A. *J. Am. Chem. Soc.* **1983**, *105*, 6021.

(31) Laskowski, E. J.; Frankel, R. B.; Gillum, W. O.; Papaefthymiou, G. C.; Renaud, J.; Ibers, J. A.; Holm, R. H. *J. Am. Chem. Soc.* **1978**, *100*, 5322.

(32) Herskovi, T.; Holm, R. H.; Weiher, J. F.; Ibers, J. A.; Averill, B. A.; Phillips, W. D. *Proc. Natl. Acad. Sci. U.S.A.* **1972**, *69*, 2437.

(33) Vaddypally, S.; Kondaveeti, S. K.; Zdilla, M. J. *Chem. Commun.* **2011**, *47*, 9696.

(34) Danopoulos, A. A.; Wilkinson, G.; Sweet, T. K. N.; Hursthouse, M. B. *J. Chem. Soc., Dalton Trans.* **1995**, 937.

(35) Verma, A. K.; Nazif, T. N.; Achim, C.; Lee, S. C. *J. Am. Chem. Soc.* **2000**, *122*, 11013.

(36) Vaddypally, S.; Kondaveeti, S. K.; Roudebush, J. H.; Cava, R. J.; Zdilla, M. J. *Chem. Commun.* **2014**, *50*, 1061.

(37) Crossland, J. L.; Zakharov, L. N.; Tyler, D. R. *Inorg. Chem.* **2007**, *46*, 10476.

(38) Schrock, R. R.; Glassman, T. E.; Vale, M. G.; Kol, M. *J. Am. Chem. Soc.* **1993**, *115*, 1760.

(39) Kuwata, S.; Mizobe, Y.; Hidai, M. *Inorg. Chem.* **1994**, *33*, 3619.

(40) Takei, I.; Dohki, K.; Kobayashi, K.; Suzuki, T.; Hidai, M. *Inorg. Chem.* **2005**, *44*, 3768.

(41) Umehara, K.; Kuwata, S.; Ikariya, T. *J. Am. Chem. Soc.* **2013**, *135*, 6754.
(42) Smith, J. M.; Lachicotte, R. J.; Holland, P. L. *J. Am. Chem. Soc.* **2003**, *125*, 15752.
(43) Sadique, A. R.; Gregory, E. A.; Brennessel, W. W.; Holland, P. L. *J. Am. Chem. Soc.* **2007**, *129*, 8112.
(44) Yonke, B. L.; Keane, A. J.; Zavalij, P. Y.; Sita, L. R. *Organometallics* **2011**, *31*, 345.
(45) Zdilla, M. J.; Dexheimer, J. L.; Abu-Omar, M. M. *J. Am. Chem. Soc.* **2007**, *129*, 11505.
(46) Cowley, R. E.; Eckert, N. A.; Vaddadi, S.; Figg, T. M.; Cundari, T. R.; Holland, P. L. *J. Am. Chem. Soc.* **2011**, *133*, 9796.
(47) Wiese, S.; McAfee, J. L.; Pahls, D. R.; McMullin, C. L.; Cundari, T. R.; Warren, T. H. *J. Am. Chem. Soc.* **2012**, *134*, 10114.
(48) Nieto, I.; Ding, F.; Bontchev, R. P.; Wang, H.; Smith, J. M. *J. Am. Chem. Soc.* **2008**, *130*, 2716.
(49) Ingemann, S.; Fokkens, R. H.; Nibbering, N. M. M. *J. Org. Chem.* **1991**, *56*, 607.
(50) Luo, Y.-R. *Handbook of Bond Dissociation Energies in Organic Compounds*; CRC Press: Boca Raton, FL, 2003.
(51) Kondaveeti, S. K.; Vaddypally, S.; Lam, C.; Hirai, D.; Ni, N.; Cava, R. J.; Zdilla, M. J. *Inorg. Chem.* **2012**, *51*, 10095.
(52) Katritzky, A. R.; Wu, J.; Verin, S. V. *Synthesis* **1995**, *1995*, 651.
(53) Carlin, R. B.; Wich, G. S. *J. Am. Chem. Soc.* **1958**, *80*, 4023.
(54) Andersen, R. A.; Faegri, K.; Green, J. C.; Haaland, A.; Lappert, M. F.; Leung, W. P.; Rypdal, K. *Inorg. Chem.* **1988**, *27*, 1782.